

Synthesis of *in-situ* encapsulated $\text{ZnS}_x\text{Se}_{1-x}/\text{ZrSiO}_4$ composite as cool pigment on ceramic tiles for energy saving

Ti Zhang^{a,b}, Yanmin Wang^{a,*}, Shanjun Ke^{b,*} and Zhidong Pan^a

^aSouth China University of Technology, Guangzhou 510640, China

^bFoshan Oceano Ceramics Co. Ltd., Foshan 528138, China

An *in-situ* encapsulated $\text{ZnS}_x\text{Se}_{1-x}/\text{ZrSiO}_4$ composite as a cool pigment on ceramic tiles was synthesized *via* soft mechano-chemical (MC) pretreatment of ZrSiO_4 precursors, high-shear homogeneous dispersing and subsequent sintering. The properties of $\text{ZnS}_x\text{Se}_{1-x}/\text{ZrSiO}_4$ composite cool pigment and solar near-infrared (NIR) reflective ceramic tiles coated with the cool pigment were investigated by X-ray diffraction (XRD), Fourier transfer infrared spectroscopy (FTIR), thermogravimetry and differential scanning calorimetry (TG-DSC), scanning electron microscopy (SEM), ultraviolet-visible-near-infrared (UV-VIS-NIR) spectroscopy and infrared irradiation image analysis. The results show that compared to ceramic tiles uncoated ($R^* = 60.07\%$), solar NIR reflective ceramic tiles coated with $\text{ZnS}_x\text{Se}_{1-x}/\text{ZrSiO}_4$ composite cool pigment have a higher solar reflectance ($R^* = 87.61\%$), indicating that the ceramic tiles coated with the cool pigment have a superior NIR reflectivity. The surface temperature of ceramic tiles coated with $\text{ZnS}_x\text{Se}_{1-x}/\text{ZrSiO}_4$ composite is 7.2°C lower than that of ceramic tile uncoated with the cool pigment. In addition, the energy saving of ceramic tiles coated the cool pigment can be achieved based on the energy simulation of solar NIR reflective ceramic tiles for ‘cool roof’ application in subtropical climate by a software named Design Builder 4.6.0.015.

Keywords: Zircon *in-situ* encapsulated, $\text{ZnS}_x\text{Se}_{1-x}$ cool pigment, Near-infrared reflectance, Solar NIR reflective ceramic tile, Energy savings, Emission reductions.

Introduction

Using ‘cool roof’ [1] products instead of conventional roofs in urban constructions provides less absorption of heat and keeps the building’s interior cool. The existing polymer materials dominate the cool roof product applications, e.g., cool coating [2-5] and cool waterproof membrane [6-8]. The industrial process of these polymer materials is simple and easy to operate. However, their weather resistance and anti-aging performance become a challenge.

Ceramic tiles coated with a cool pigment enamel layer could give an innovative approach [9-13]. This approach may complement the cool roof products [14]. Ceramic-based cool roof products [15-17] (e.g., ceramic tiles, clay roof tiles, etc.) possess high mechanical properties, fire resistance, and excellent chemical and physical durability [18]. Conventional ceramic tiles [19, 20] usually consist of three layers, i.e., ceramic substrates, thin engobe and pigmented overglaze [21, 22]. To meet the application demand for cold roof products with different colors and decorative effects, multicolor inorganic pigments with a high NIR reflectance

were added into the ceramic glaze to prepare cool ceramic tiles [23-27]. The dense glaze layer on the surface of ceramic tiles has a certain antifouling ability, which can reduce the surface pollution caused by weathering and scaling.

Ferrari et al. [28] prepared a white ceramic tile with a high total solar reflectance (TSR) by coating ZrSiO_4 glaze on the surface of ceramic substrates. They found that the TSR values of ceramic tiles are related to its microstructure, mineral composition and surface roughness. Levinson et al. [29] proposed a manufacturing method to prepare multi-colored overglaze and coating onto the clay tile surfaces as non-white surface ceramic tiles with a high NIR reflectance using clay tiles as base materials. The cool ceramic tile products can be industrially produced *via* only adjusting the formula of ceramic tiles. Therefore, it is more cost-effective to prepare cool ceramic tile products by coating near-infrared reflective glaze on the surface of ceramic substrates. The development of cool ceramic tiles will become a promising research field.

In this paper, the application and energy saving of potential cool ceramic pigments (e.g. zircon *in-situ* encapsulated $\text{ZnS}_x\text{Se}_{1-x}$ cool pigment) on ceramic tiles were evaluated. The annual energy and emission savings of applying solar NIR reflective ceramic tiles in subtropical regions were simulated by a software named Design Builder based on the dynamic energy

*Corresponding author:
Tel : +86 20 87114883
Fax: +86 20 87110273
E-mail: wangym@scut.edu.cn (Y. Wang), sjkescut@163.com (S. Ke)

consumption simulation.

Experimental

Materials

Tetraethyl orthosilicate (TEOS, 98% purity), zirconium oxychloride ($\text{ZrOCl}_2 \cdot 8\text{H}_2\text{O}$, 98% purity), lithium fluoride (LiF, 99% purity), zinc sulfate heptahydrate ($\text{ZnSO}_4 \cdot 7\text{H}_2\text{O}$, 99.5% purity), copper sulfate pentahydrate ($\text{CuSO}_4 \cdot 5\text{H}_2\text{O}$, 99% purity), indium sulfate ($\text{In}_2(\text{SO}_4)_3$, 99% purity), sodium sulfide nonahydrate ($\text{Na}_2\text{S} \cdot 9\text{H}_2\text{O}$, 98% purity), selenium (Se, 99.9% purity, Umicore Group, Belgium), sodium hydroxide flakes (NaOH, 97% purity) were used as raw materials. Chemicals were purchased from Shanghai Macklin Biochemical Co. Ltd., China.

Synthesis of *in-situ* encapsulated $\text{ZnS}_x\text{Se}_{1-x}/\text{ZrSiO}_4$ composite cool pigment

Zircon-based *in-situ* encapsulated pigment (i.e., $\text{ZnS}_x\text{Se}_{1-x}/\text{ZrSiO}_4$ composite) was prepared by soft mechano-chemical pretreatment of ZrSiO_4 precursors [30], high-shear homogeneous dispersing and subsequent sintering. Fig. 1 shows the preparation process of $\text{ZnS}_x\text{Se}_{1-x}/\text{ZrSiO}_4$ composite as a cool pigment.

For preparation of $\text{ZnS}_x\text{Se}_{1-x}/\text{ZrSiO}_4$ (labeled as ZS/ZrSiO_4) composite cool pigment, $\text{ZnS}_x\text{Se}_{1-x}$ (labeled as ZS) precursor particles were synthesized *via* co-precipitation reaction, the optimum process of $\text{ZnS}_x\text{Se}_{1-x}$ precursor synthesis was described in a previous work [31] and the atomic ratio of Zn:S:Se is 1.00:0.35:0.65. Afterwards, $\text{ZnS}_x\text{Se}_{1-x}$ precursor particles were mixed with soft mechano-chemical pretreated ZrSiO_4 precursors in a model D-500 high-shear homogeneous dispersing emulsifier (Wiggins Co., Ltd., Germany) at a rotational speed of 20,000 rpm. ZS/ZrSiO_4 precursors were calcined in N_2 atmosphere at 700 °C for 60 min.

Preparation of solar NIR reflective ceramic tiles

The preparation process of solar NIR reflective ceramic tiles consists of two steps, i.e., ceramic substrates preparation and solar NIR reflective glaze coating on ceramic substrate surfaces.

The ceramic substrate comprises ceramic body and ceramic engobe with the formula according to GB/T 4100-2015 (Ceramic Tile), PRC. The sintering process of solar NIR reflective ceramic tiles is a double-firing process (i.e., the ceramic substrates are sintered at 1,100~1,200 °C, and then the ceramic tiles with solar NIR reflective glaze are sintered at 1,050~1,150 °C). The chemical compositions of ceramic bodies and engobe are shown in Tables A.1 and A.2.

Solar NIR reflective glaze comprises low-temperature frit and NIR reflective pigment (i.e., $\text{ZnS}_x\text{Se}_{1-x}/\text{ZrSiO}_4$ composite). The chemical composition of low-temperature frit is shown in Table A.3. $\text{ZnS}_x\text{Se}_{1-x}/\text{ZrSiO}_4$ composite cool pigment and low-temperature frit were put in an agate mortar and mixed evenly (the mass ratio of pigment to frit is 10:90), then a certain amount of anhydrous ethanol was added into and mixed with above powder to form a slurry and coated on the ceramic substrate. After drying overnight, the solar NIR reflective ceramic tiles were calcined at 1,050 °C for 30 min.

Energy simulation

The simulations were performed in subtropical climate (see Fig. 2) by using a graphical user interface for EnergyPlus which named Design Builder 4.6.0.015.

A six-story residential house (see Fig. 3) was considered for simulation. The total building area is 3,158.18 m². The prototype was modeled with two different roof albedos, representing as-prepared solar NIR reflective ceramic tiles (solar radiation absorption coefficient $\rho = 0.3$) and cement wall ($\rho = 0.7$), respectively. Geography and climate of Guangzhou, China see Table 1. Assumptions of parameters used to compute energy cost, and emission savings see Table 2.

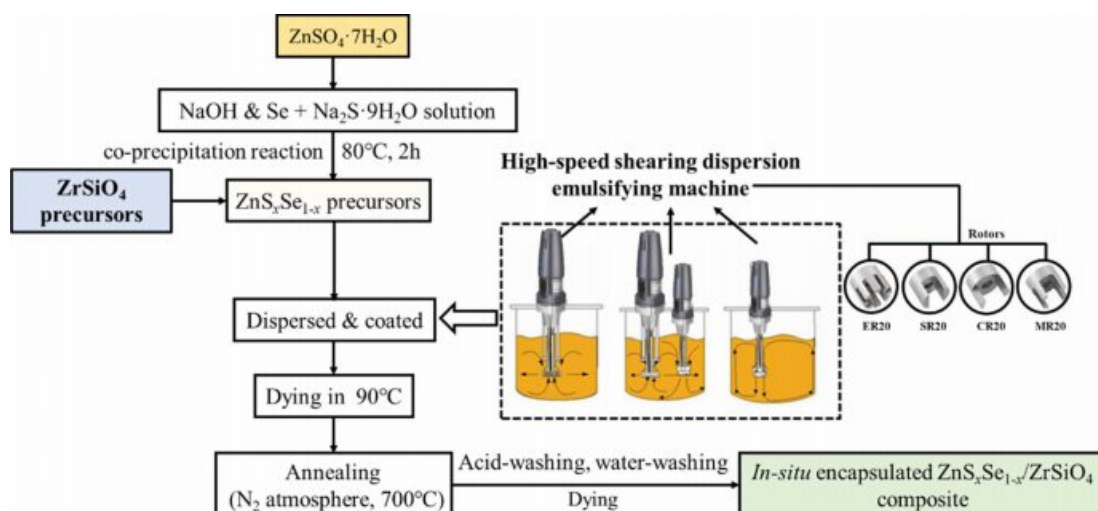


Fig. 1. Preparation process of $\text{ZnS}_x\text{Se}_{1-x}/\text{ZrSiO}_4$ composite cool pigment.

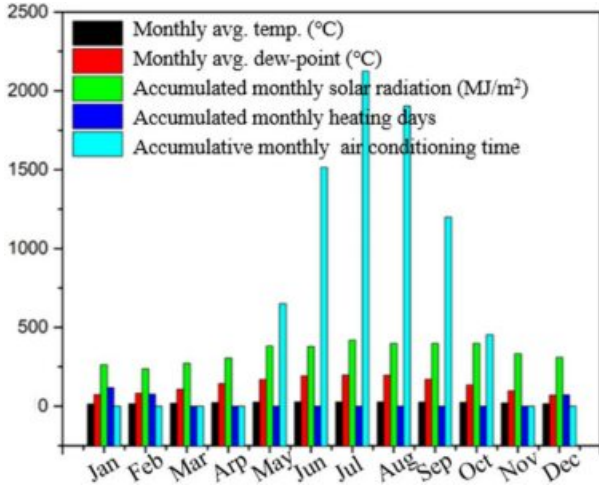


Fig. 2. Standard annual weather data in subtropical climate.

Table 1. Summer and winter average temperatures and solar irradiance of subtropical climate

Climate zone	Subtropical climate (Hot summer/warm winter)
Summer avg. temp. (°C)	28.3
Winter avg. temp. (°C)	14.7
Annual avg. solar irradiation (W/m ²)	130

Characterizations

The crystal structure of samples were determined by an X-ray diffractometer (XRD, PANalytical B.V., the Netherlands) with Cu K α radiation ($\lambda = 1.5406 \text{ \AA}$). The Fourier transform infrared spectra of samples were recorded on a Fourier infrared spectrometer (FTIR, Thermo Fisher Scientific Co. Ltd., USA) in a frequency range of 400-4,000 cm⁻¹. The thermal properties of

Table 2. Assumptions of parameters used to compute energy cost, and emission savings from heating and cooling load savings

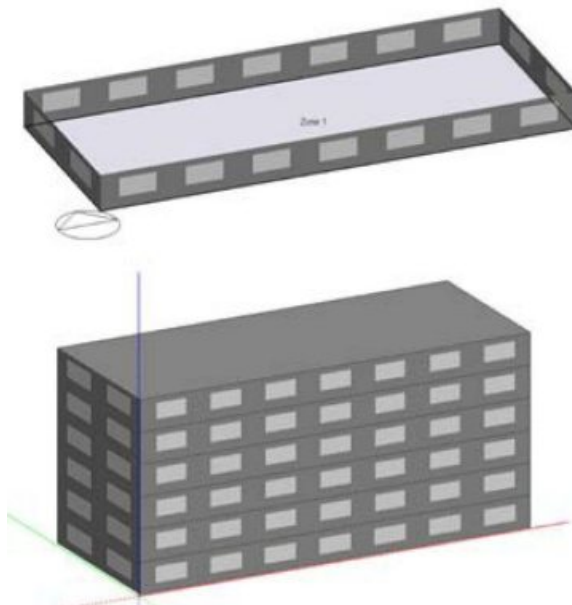
Calculation Parameters		Values
Coefficient of performance (COP)	Heating COP	3.5
	Cooling COP	3.3
Electricity price (RMB/kW·h)	Industrial and commercial electricity	0.7752
	Residential electricity	0.5908
Electricity emission factor	CO ₂ (kg/kW·h)	0.9344
	NO _x (g/kW·h)	3.7
	SO ₂ (g/kW·h)	9.1

samples were measured by a model STA449C/3/MFC/G thermogravimeter and differential scanning calorimeter (TG-DSC, Netzsch Instruments Ltd., Germany) in air at a heating rate of 10 °C/min with $\alpha\text{-Al}_2\text{O}_3$ as a reference. The microstructures of samples were characterized by a scanning electron microscope (SEM, Carl Zeiss AG, Germany), equipped with energy-dispersive X-ray analysis. The L*a*b* color parameters of samples were measured by a reflection differential colorimeter (X-Rite Co., USA). The UV-vis-NIR diffuse reflectance spectra of samples were acquired in a high-resolution double-monochromator spectrophotometer (PerkinElmer Co. Ltd., USA). The NIR solar reflectance (R^*) was calculated in accordance with the ASTM standard G159-98,

$$R^* = \frac{\int_{700}^{2500} r(\lambda)i(\lambda)d(\lambda)}{\int_{700}^{2500} i(\lambda)d(\lambda)} \tag{1}$$

where $r(\lambda)$ is the spectral reflectance ($\text{W}\cdot\text{m}^{-2}$) and $i(\lambda)$ is the solar spectral irradiance ($\text{W}\cdot\text{m}^{-2}\cdot\text{nm}^{-1}$) obtained from the ASTM standard G159-98.

For evaluating thermal performance of the solar NIR



Building Area

	Area [m2]
Total Building Area	3158.18
Net Conditioned Building Area	3158.18
Unconditioned Building Area	0.00



Fig. 3. Design Builder simulation building model.

reflective ceramic tiles, an infrared thermal camera (FLIR Systems Inc., USA) was used to observe the surface temperature distribution of ceramic tiles. Fig. A.1 shows the experimental device to measure the temperature difference of ceramic tiles.

Result and Discussion

ZnS_xSe_{1-x}@ZrSiO₄ composite cool pigment

Fig. 4 shows XRD patterns and FTIR spectra of ZS@ZrSiO₄ composite cool pigment sintered at 700 °C. The diffraction peaks of ZS@ZrSiO₄ composite mainly consist of zircon phase (ZrSiO₄, JCPDS card 06-0266) with high crystallinity degree, and a small amount of ZnSe (JCPDS card 37-1463) are detected (see Fig. 4(a)). It indicates that the coating process does not change the crystalline structure of ZnS_xSe_{1-x} pigment (i.e., ZnSe, cubic zinc-blende structure, space group of F-43m(216)) [31].

Fig. 4(b) shows the FT-IR spectra of ZS@ZrSiO₄ composite. The bands located at 899 cm⁻¹ are ascribed to Si-O-Zr characteristic vibrations [32], which is similar to the FTIR spectrum of ZrSiO₄. Besides, the characteristic major peaks of ZnS appear at 1,110 cm⁻¹

and 672 cm⁻¹ [33], and the bands appeared at 553 and 1,639 cm⁻¹ belong to Zn-Se vibrations [34], indicating that the ZS@ZrSiO₄ composite cool pigment are effectively coated by ZrSiO₄. The thermal stability of ZnS_xSe_{1-x}@ZrSiO₄ composite is superior to ZnS_xSe_{1-x} pigment [31, 35] (see Fig. 5) for ceramic glazes and tiles.

The mechanism diagram for the formation of ZrSiO₄ *in-situ* encapsulated ZnS_xSe_{1-x} pigment see Fig. A.2. The chemical and coloration stability of ZS@ZrSiO₄ composite cool pigment were tested according to the PRC National Standard GB/T 3810.13-2016 [36]. The as-prepared composite cool pigments were soaked in H₂O and 6 wt.% HNO₃, NaOH, C₂H₅OH, respectively. The color coordinates of ZS@ZrSiO₄ composite cool pigments treated in different solutions see Tables 3. The ΔE represented the total color difference between untreated and treated pigments.

Ceramic tile coated with ZS@ZrSiO₄ composite cool pigment

Photographs of as-prepared solar NIR reflective ceramic tiles see Fig. 6. All enameled samples with ZS@ZrSiO₄ composite cool pigment exhibit a homo-

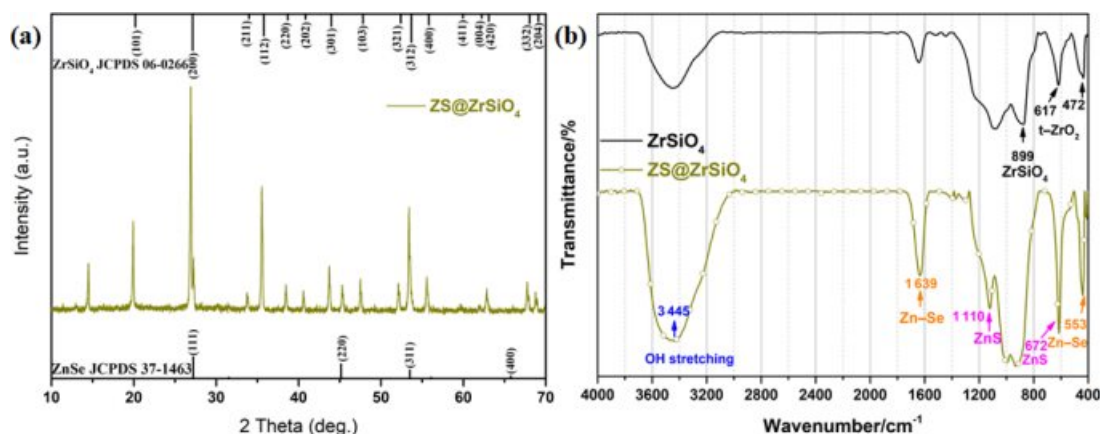


Fig. 4. XRD patterns (a) and FTIR spectra (b) of ZS@ZrSiO₄ composite cool pigment sintered at 700 °C.

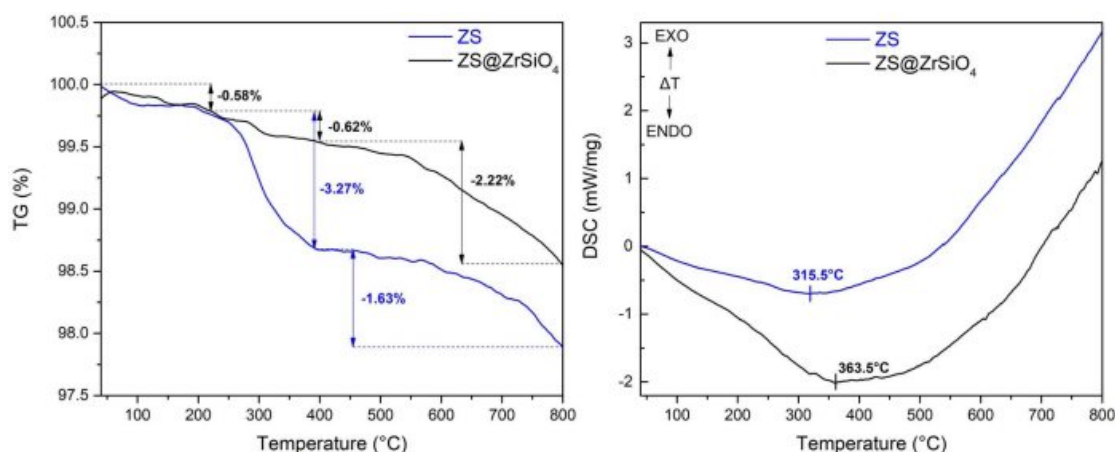

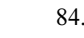
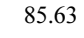
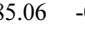
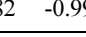


Fig. 5. TG-DSC curves of ZS and ZS@ZrSiO₄ composite cool pigment.

Table 3. The color coordinates of ZS@ZrSiO₄ encapsulation pigment treated in different solutions

Different solutions	CIE				Images
	L*	a*	b*	ΔE	
Before treatment	84.07	-1.89	29.53	–	
H ₂ O	84.38	-1.36	29.36	1.08	
HNO ₃	85.63	-0.67	28.47	2.25	
NaOH	85.06	-0.99	28.95	1.38	
C ₂ H ₅ OH	84.82	-0.99	29.28	1.17	

geneous yellow hue, and the yellow chromaticity of samples enhanced with the increasing of coating times. It means that the as-prepared ZS@ZrSiO₄ composite cool pigment has high thermal stability and tinting strength, which makes them suitable for ceramic decoration.

The color coordinates of solar NIR reflective ceramic tiles see Table 4. The L* values of uncoated glaze-white are 90.39, indicating that the as-prepared ceramic substrates have excellent whiteness. In the enameled samples with ZS@ZrSiO₄ composite, the b* value of enameled samples rises from 27.66 to 41.11 with the increasing of coating times, and the color of all of the enameled samples are brighter yellow.

The cross-section of enameled sample with ZS@ZrSiO₄ composite cool pigment and coated for 3 times (i.e., ZS@ZrSiO₄ glaze-3) was observed by SEM, and the thickness of glaze layer is 50–60 μm (see Fig. 7(a)). Fig. 7(b) shows the surface of ZS@ZrSiO₄ glaze-3 sample. The glaze sample surface is rough and possesses

Table 4. The color coordinates of solar NIR reflective ceramic tiles

Glazes samples	CIE			
	L*	a*	b*	
Uncoated glaze-white	90.39	1.74	4.85	
ZS@ZrSiO ₄ glazes	1-time coating	87.61	-1.40	27.66
	2-time coating	86.03	-2.04	32.63
	3-time coating	85.90	-1.91	37.80
	4-time coating	84.86	-1.56	38.48
	5-time coating	85.87	-1.28	41.11

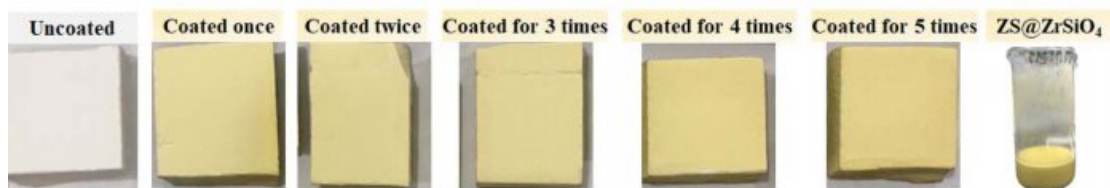
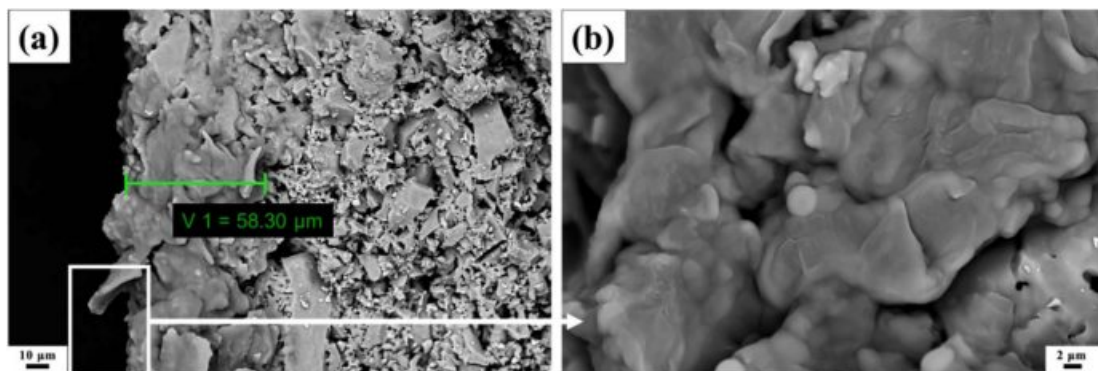
a small amount of pin-hole defects.

To evaluate the thermal insulation performance of solar NIR reflective ceramic tiles, Fig. 8 shows the comparison of NIR reflectance of the ceramic substrates (i.e., uncoated glaze-white) and enameled samples with composite cool pigment (i.e., ZS@ZrSiO₄ glaze-3).

Clearly, the NIR reflectance of ceramic substrates is significantly lower in the NIR wavelength range of 1,850–2,050 nm. Because the white engobe coated on the ceramic substrate surface is a matte glaze, which has lower reflectivity compared with gloss glaze or transparent glaze [28].

The NIR solar reflectance of ZS@ZrSiO₄ glaze-3 is 87.61%, higher than that of uncoated glaze-white ($R^* = 60.07$), indicating that solar NIR reflective yellow ceramic tiles have excellent NIR reflectivity (see Table 5).

The radiant range of light energy or electromagnetism from the sun is wide (300–2,500 nm), therefore, there is only a part of the solar spectrum that can be seen by

**Fig. 6.** Photographs of as-prepared solar NIR reflective ceramic tiles.**Fig. 7.** SEM micrographs of sample ZS@ZrSiO₄ glaze-3: (a) cross-section image and (b) surface of ceramic glaze.

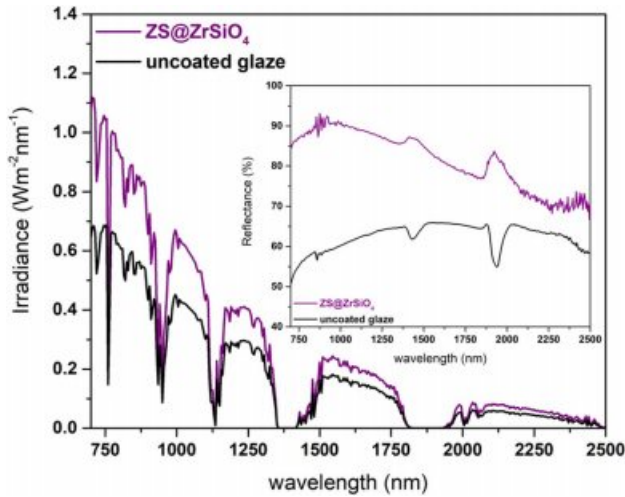


Fig. 8. Solar reflectance spectra of solar NIR reflective ceramic glazes samples (NIR reflectance in the inset).

Table 5. The NIR reflective properties of solar NIR reflective ceramic tiles, compared to those of uncoated glaze-white

	NIR solar reflectance (%)	TSR (%)
ZS@ZrSiO ₄ glaze-3	87.61	70.20
uncoated glaze-white	60.07	61.34

human eyes. The light irradiated on an object occurs various phenomena, such as surface reflection, selective absorption or transmission.

Suppose the initial light energy in the plane perpendicular to the propagation direction of light (i.e., Light fluence rate) is I_O , the transmitted light energy of the object illuminated by light is I_T , and the reflected light energy is I_R , absorbed light energy is I_A , then there is

$$I_O = I_T + I_R + I_A \quad (2)$$

$$T + R + A = 1 \quad (3)$$

$$T = I_T/I_O \quad (4)$$

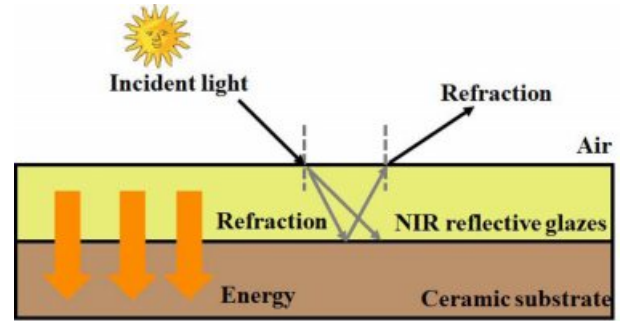


Fig. 10. The cross section of solar NIR reflective ceramic tiles and optical and thermodynamic analysis.

$$R = I_R/I_O \quad (5)$$

$$A = I_A/I_O \quad (6)$$

where A , T , and R are absorption coefficient, transmission coefficient and reflection coefficient, respectively.

In a ceramic structure, the transmission effect is negligible ($T \approx 0$) when light incidents from the air. Therefore, the intensity of light reflection on ceramic glaze surface determines the light energy entering the tile (see Fig. 9). Shining on the surface of the ceramic glaze is followed by the increasing heat energy conducted into the building. This achieves the conversion of optical phenomena into thermodynamic process.

Schabbach et al. [9] investigated the TSR and optical properties of pigmented glazed ceramic tiles. The results show that, there is high absorption of radiation in the near-infrared region for some glazes, which means most of the ceramic tiles in use show ‘non-cool’ surfaces [37]. However, the solar radiation reflecting can be achieved by coating NIR reflective glaze layer on ceramic substrates.

For thermal performance analysis, the solar NIR reflective ceramic tiles were exposed to infrared lamps, and the temperature distribution of the coating surface was visually depicted (see Fig. A.1). As shown in Fig. 11(a), the surface temperature of enameled samples

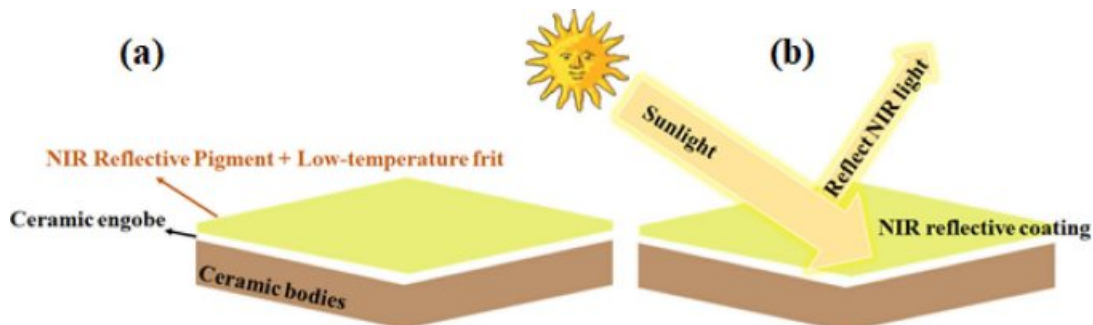


Fig. 9. Schematic diagram of spraying of pigmented glaze on ceramic substrate surface (a) and structural diagram of solar NIR reflective glaze coating on ceramic substrate surfaces (b).

with ZS@ZrSiO₄ composite cool pigment decrease with the increasing of coating times, indicating the outstanding thermal insulation performance of solar NIR reflective ceramic tiles.

Compared with enameled samples with ZS@ZrSiO₄ composite cool pigment, the uncoated glaze-white sample absorbed the most infrared radiation after exposing to the radiation for 10 min, resulting in the surface temperature rising to 50.1 °C (see Fig. 11(b)).

Libbra et al. [37] found that common ceramic tiles have a relatively low solar reflectance (i.e., smaller than 0.30-0.40), which means, it is necessary to optimizing the NIR reflective properties of ceramic tiles, especially the pigmented enamel layer on the ceramic substrates.

According to the temperature difference of 5.1-7.2 °C for enameled samples with ZS@ZrSiO₄ composite cool pigment (see Table 6), solar NIR reflective ceramic tiles can be a novel ceramic-based cool roof product for building surface cooling and energy saving.

Table 6. The maximum surface temperature of solar NIR reflective ceramic glazes samples after exposing to the radiation for 10 min

	Uncoated glaze-white	ZS@ZrSiO ₄ glazes		
		1-time coating	3-time coating	5-time coating
T _{max} /°C	50.1	45.0	43.4	42.9
ΔT/°C	-	5.1	6.7	7.2

Energy-saving estimation

The energy saving of ZS@ZrSiO₄ composite cool pigment on ceramic tiles were evaluated by Design Builder. Reducing solar radiation absorption coefficient to 0.3 (i.e., solar NIR reflective ceramic tiles) from 0.7 (i.e., cement wall) decreases the annual cooling load of the building from 651647.48 kWh to 644894.07 kWh, with a saving of 6753.41 kWh, while reducing its annual cooling load by 2.138 kWh/m² (see Fig. 12). Meantime, the annual heating load increases from 1757.42 kWh to 1876.93 kWh, increasing its annual cooling load by 0.038 kWh/m² (see Table 7).

According to the Electricity price list of Guangzhou, China (effective from July 1, 2018), energy cost savings in the industrial and commercial building is 1.63 RMB/m² and in the residential building is 1.24 RMB/m² (see Table 8), and the emission reductions of CO₂, NO_x and SO₂ are 1.24 kg/m², 7.77 g/m² and 148.48 g/m², respectively.

Table 7. Annual heating and cooling load savings in simulated building

Annual cooling load saving (kWh)	Annual heating load saving (kWh)	Annual cooling load saving per unit area (kWh/m ²)	Annual heating load saving per unit area
6753.41	-119.51	2.138	-0.038

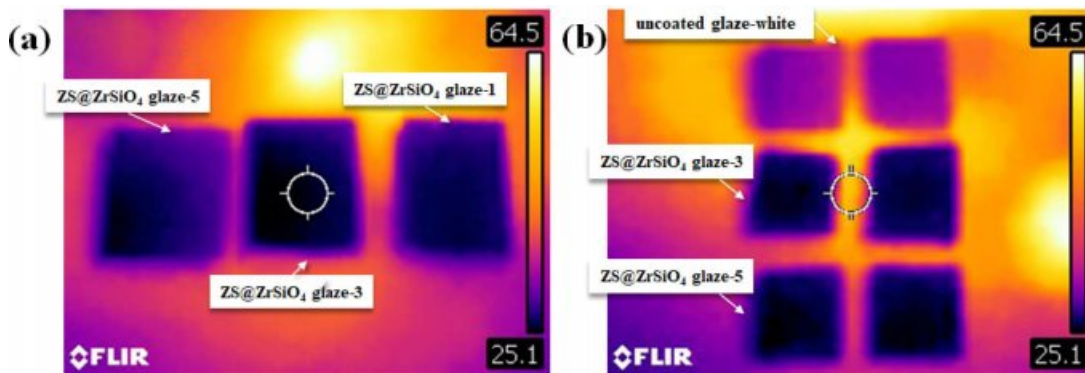


Fig. 11. Infrared irradiation images of ZS@ZrSiO₄ glazes (a) and uncoated glaze-white with solar NIR reflective ceramic tiles (b).

(a)

	Electricity [kWh]	Natural Gas [kWh]	Additional Fuel [kWh]	District Cooling [kWh]	District Heating [kWh]	Water [m3]
Heating	0.00	0.00	0.00	0.00	1757.42	0.00
Cooling	0.00	0.00	0.00	651647.48	0.00	0.00

(b)

End Uses

	Electricity [kWh]	Natural Gas [kWh]	Additional Fuel [kWh]	District Cooling [kWh]	District Heating [kWh]	Water [m3]
Heating	0.00	0.00	0.00	0.00	1876.93	0.00
Cooling	0.00	0.00	0.00	644894.07	0.00	0.00

Fig. 12. Annual district cooling load and heating load calculated by Design Builder, (a) cement wall and (b) solar NIR reflective ceramic tiles.

Table 8. Annual energy cost and emission savings in simulated building

Building types	Energy cost savings (RMB/m ²)	CO ₂ savings (kg/m ²)	NO _x savings (g/m ²)	SO ₂ savings (g/m ²)
Industrial and commercial building	1.63	1.24	7.77	148.48
Residential building	1.24			

Conclusion

To improve the thermal stability of ZnS_xSe_{1-x} pigment, zircon-based *in-situ* encapsulated pigment (i.e., ZnS_xSe_{1-x}@ZrSiO₄) were prepared with the assistance of soft mechano-chemical activation of ZrSiO₄ precursors *via* high-shear homogeneous dispersing and subsequent sintering. The as-synthesized ZS@ZrSiO₄ composite cool pigment possessed superior chromatic performance, high-temperature thermal stability and chemical stability. It is expected to be used as a thermal insulating coating material on ceramic tiles.

For thermal performance analysis, the as-prepared solar NIR reflective ceramic tiles were exposed to infrared lamps, and the surface temperature distribution of the coating was visually depicted by an infrared thermal camera. According to the temperature difference of 5.1-7.2 °C for enameled samples with ZS@ZrSiO₄ composite cool pigment, solar NIR reflective ceramic tiles could be a novel ceramic-based cool roof product for building surface cooling and energy saving.

The application and energy saving of as-prepared solar NIR reflective ceramic tiles were evaluated. The annual building energy performance of applying solar NIR reflective ceramic tiles was simulated by Design Builder. The annual cooling load saving per unit area of building was 2.138 kWh/m², the energy cost savings of building was 1.24-1.63 RMB/m², and the emission reductions of CO₂, NO_x and SO₂ are 1.24 kg/m², 7.77 g/m² and 148.48 g/m², respectively. The simulations indicated that substituting solar NIR reflective ceramic tiles for cement walls could yield positive annual load, source energy, energy cost, CO₂, NO_x and SO₂ savings in subtropical regions (e.g., Guangzhou, China).

The ‘cool roof’ solution for solar NIR reflective

ceramic tiles had excellent energy-saving performance, promising popularization and application in public and residential buildings.

Acknowledgements

This work was supported by the China Postdoctoral Science Foundation (No. 2021M690722) and Guangdong Basic and Applied Basic Research Foundation (No. 2021A1515110487).

Appendix A.

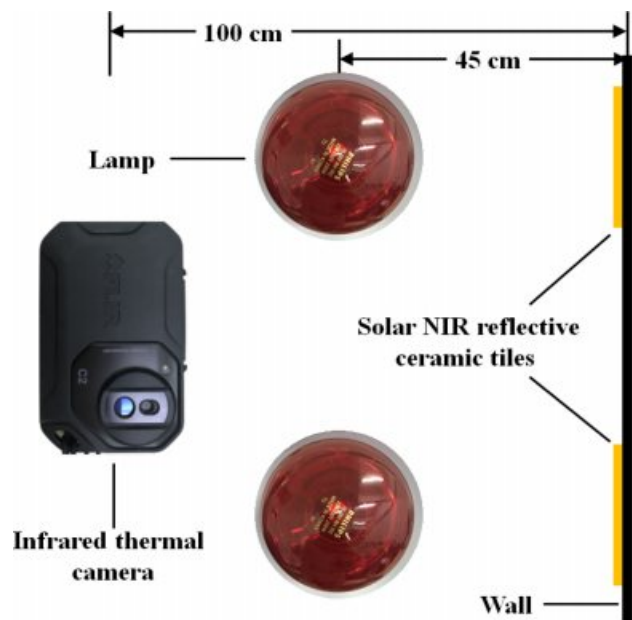


Fig. A.1. Schematic diagram of experimental apparatus for thermal image analysis and temperature distribution test

Table A.1. Chemical composition of ceramic bodies (wt.%)

SiO ₂	Al ₂ O ₃	Fe ₂ O ₃	CaO	MgO	K ₂ O	Na ₂ O	Ignition loss (I.L)
64.50	16.66	1.28	6.72	0.94	2.22	0.87	6.48

Table A.2. Chemical composition of ceramic engobe (wt.%)

SiO ₂	Al ₂ O ₃	Fe ₂ O ₃	CaO	MgO	K ₂ O	Na ₂ O	ZnO	ZrO ₂	B ₂ O ₃	BaO	TiO ₂	I.L
56.90	11.28	0.24	2.93	13.53	1.75	0.30	2.02	7.66	0.78	0.52	0.07	1.49

Table A.3. Chemical composition of low-temperature ceramic frit (wt.%)

SiO ₂	B ₂ O ₃	MgO	ZrO ₂	K ₂ O	Na ₂ O	Ca ₃ (PO ₄) ₂	CaCO ₃	I.L
28.5	42.3	2.5	3.5	2.5	7.5	1.5	11.7	1.36

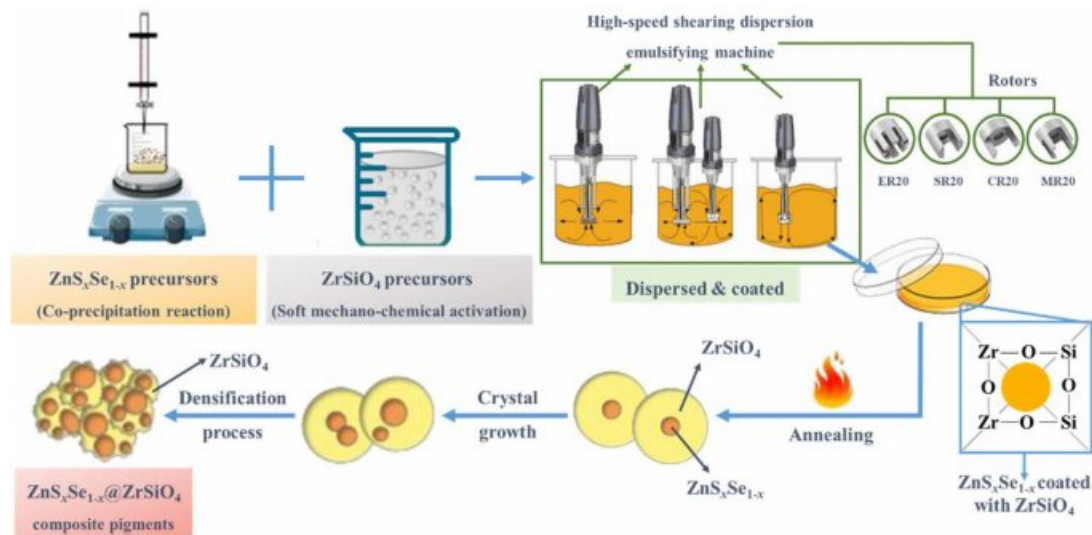


Fig. A.2. The mechanism diagram for the formation of ZS@ZrSiO₄ composite cool pigment

References

- M. Ullah, H.J. Kim, J.G. Heo, D.K. Roh, and D.S. Kim, *J. Ceram. Process. Res.* 20 (2019) 86-91.
- M. Suwan, P. Premjit, P. Thavorniti, P. Kidkhunthod, and S. Supothina, *J. Ceram. Process. Res.* 18 (2017) 10-15.
- C. Zhu, W. Lin, L. Chen, J. Lv, J. Zhang, and J. Feng, *Sol. Energy Mater. Sol. Cells.* 199 (2019) 129-135.
- N. Xie, H. Li, W. Zhao, C. Zhang, B. Yang, H. Zhang, and Y. Zhang, *Build. Environ.* 163 (2019) 106334.
- T. Kolás, A. Røyset, M. Grandcolas, M.T. Cate, and A. Lacau, *Sol. Energy Mater. Sol. Cells* 196 (2019) 94-104.
- C. Piselli, V.L. Castaldo, and A.L. Pisello, *Sol. Energy* 192 (2019) 106-119.
- A.L. Pisello, E. Fortunati, C. Fabiani, S. Mattioli, F. Dominici, L. Torre, L.F. Cabeza, and F. Cotana, *Sol. Energy Mater. Sol. Cells* 160 (2017) 34-42.
- A.L. Pisello, E. Fortunati, S. Mattioli, L.F. Cabeza, C. Barreneche, J.M. Kenny, and F. Cotana, *Energy Build.* 112 (2016) 40-48.
- L.M. Schabbach, D.L. Marinovski, S. Güths, A.M. Bernardin, and M.C. Fredel, *Sol. Energy* 159 (2018) 113-124.
- Z. Li, M. Zhao, J. Zeng, C. Peng, and J. Wu, *Sol. Energy* 153 (2017) 623-627.
- E. Enríquez, V. Fuertes, M.J. Cabrera, J. Soares, D. Muñoz, and J.F. Fernández, *Sol. Energy* 149 (2017) 114-124.
- G.M. Revel, M. Martarelli, M. Emiliani, A. Gozalbo, M.J. Orts, M.Á. Bengochea, L. Guaita Delgado, A. Gaki, A. Katsiapi, M. Taxiarchou, I. Arabatzis, I. Fasaki, and S. Hermanns, *Sol. Energy* 105 (2014) 770-779.
- G.M. Revel, M. Martarelli, M. Emiliani, L. Celotti, R. Nadalini, A.D. Ferrari, S. Hermanns, and E. Beckers, *Sol. Energy* 105 (2014) 780-791.
- I. Tatar, N. Ediz, and A. Aydin, *J. Ceram. Process. Res.* 16 (2015) 81-88.
- N.T. Tran, D.V.Q. Nguyen, V.M.H. Ho, X.T. Dang, and N.Q. Tran, *J. Ceram. Process. Res.* 18 (2017) 366-372.
- S.U. Bayca, T. Batar, E. Sayin, O. Solak, and B. Kahraman, *J. Ceram. Process. Res.* 9 (2008) 118-122.
- J.G. Song, F. Wang, X.B. Bai, D.M. Du, Y.Y. Ju, M.H. Xu, and G.C. Ji, *J. Ceram. Process. Res.* 12 (2011) 357-360.
- C. Ferrari, A. Muscio, and C. Siligardi, *Procedia Eng.* 169 (2016) 400-407.
- N.M. Khalil, M.M.S. Wahsh, and A. Gaber, *J. Ceram. Process. Res.* 17 (2016) 478-484.
- J. García-Ten, E. Monfort, P. Gomez, and S. Gomar, *J. Ceram. Process. Res.* 7 (2006) 75-82.
- J.H. Lee, H.J. Hwang, J.W. Kwon, J.H. Kim, K.T. Hwang, and K.S. Han, *J. Ceram. Process. Res.* 20 (2019) 127-132.
- F. Karimi, S. Baghshahi, M.N. Khezrabad, and N. Riahi-Noori, *J. Ceram. Process. Res.* 20 (2019) 357-362.
- J. Zou and P. Zhang, *Ceram. Int.* 46 (2020) 3490-3497.
- X. Huang, D. Liu, N. Li, J. Wang, Z. Zhang, and M. Zhong, *Sol. Energy* 202 (2020) 164-170.
- J. Zou, T. Zhang, and X. He, *Mater. Lett.* 248 (2019) 173-176.
- J. Zou and Z. Yu, *Sol. Energy Mater. Sol. Cells* 199 (2019) 99-107.
- H.N. Deepak, K.S. Choudhari, S.A. Shivashankar, C. Santhosh, and S.D. Kulkarni, *J. Alloys Compd.* 785 (2019) 747-753.
- C. Ferrari, A. Libbra, A. Muscio, and C. Siligardi, *Ceram. Int.* 39 (2013) 9583-9590.
- R. Levinson, P. Berdahl, H. Akbari, W. Miller, I. Joedicke, J. Reilly, Y. Suzuki, and M. Vondran, *Sol. Energy Mater. Sol. Cells* 91 (2007) 304-314.
- T. Zhang, Z. Pan, and Y. Wang, *J. Sol-Gel Sci. Technol.* 84 (2017) 118-128.
- T. Zhang, Y. Wang, and Z. Pan, *Ceram. Int.* 44 (2018) 18851-18862.
- C. Pecharrromán, M. Ocaña, P. Tartaj, and C.J. Serna, *Mater. Res. Bull.* 29 (1994) 417-426.
- M. Ahadi, M. Saber Tehrani, P. Aberoomand Azar, and S. Waqif Husain, *Int. J. Environ. Sci. Te.* 13 (2016) 2797-2804.
- K. Petzke, *Physica B* 273-274 (1999) 866-869.
- T. Zhang, Y. Wang, and Z. Pan, *Sol. Energy* 184 (2019) 570-583.
- P.N.S. PRC National Standard, GB/T 3810.13-2016 (2016) p.1-5.
- A. Libbra, L. Tarozzi, A. Muscio, and M.A. Corticelli, *Opt. Laser Technol.* 43 (2011) 394-400.